

# Understanding Electron Transfer on the Single-Molecule Level

James O. Thomas<sup>\*†a,b</sup>, Bart Limburg<sup>\*†a,b</sup>, Jakub K. Sowa<sup>†b</sup>, Kyle Willick<sup>c</sup>, Jonathan Baugh<sup>c</sup>, G. Andrew D. Briggs<sup>b</sup>, Erik M. Gauger<sup>d</sup>, Harry L. Anderson<sup>\*a</sup> and Jan A. Mol<sup>\*b,e</sup>

\* Correspondence should be addressed to james.thomas@chem.ox.ac.uk, bart.limburg@chem.ox.ac.uk, harry.anderson@chem.ox.ac.uk, jan.mol@materials.ox.ac.uk

† These authors contributed equally.

<sup>a</sup> Department of Chemistry, University of Oxford, Chemistry Research Laboratory, Oxford OX1 3TA, UK.

<sup>b</sup> Department of Materials, University of Oxford, Parks Road, Oxford OX1 3PH, UK.

<sup>c</sup> Institute for Quantum Computing, University of Waterloo, Waterloo, ON N2L 3G1, Canada.

<sup>d</sup> SUPA, Institute of Photonics and Quantum Sciences, Heriot-Watt University, Edinburgh EH14 4AS, UK.

<sup>e</sup> Department of Physics, Queen Mary University, London, E1 4NS, UK

**Electron-transfer reactions are ubiquitous in chemistry, however, there are still gaps in the fundamental understanding of electron transfer at the molecular level, particularly the degree to which the nuclear dynamics that accompany the process straddle the quantum-classical boundary. Here, we use single-molecule transistors to study the mechanism of electron transfer at a range of temperatures. We observe a simultaneous breakdown of quantum coherent Landauer and semi-classical Marcus theory. We propose a theoretical model based on a quantum master equation, and demonstrate that it quantitatively describes rates of electron transfer in single molecules. We show that nuclear tunnelling enhances the rates of low-energy electron transfer, and demonstrate that the rates are sensitive to both the outer and inner-sphere environmental interactions. We find that the nuclear dynamics accompanying electron transfer must be treated quantum mechanically as the quantitative validity of Marcus theory is expected to occur at temperatures exceeding 298 K.**

A quantitative understanding of electron-transfer reactions is of fundamental importance in areas such as photochemistry, electrochemistry and catalysis. Furthermore these reactions are essential to many biological processes<sup>1,2</sup> and quantum technologies,<sup>3,4</sup> and are at the core of challenges relating to energy conversion.<sup>5,6</sup> Off-resonant molecular charge transport, in which the molecular energy levels are far from the Fermi level of the

electrodes, is well described by non-interacting scattering approaches. These approaches are epitomised by Landauer theory, in which the molecule is reduced to a scattering centre with an energy dependent transmission spectrum.<sup>7</sup> However, when one of the molecular energy levels of a weakly coupled molecule falls into the bias window between the Fermi levels of the electrodes, sequential electron transfers take place: an electron tunnelling from the source electrode localises on the molecule for a short time before tunnelling into the drain. As both the electron occupancy and the equilibrium geometry of the molecule and its local environment change upon an electron transfer, the electron-electron and electron-vibration interactions can no longer be ignored. Semi-classical Marcus theory accounts for these interactions, and describes the transport as a series of oxidation and reduction processes with rates determined by nuclear reorganisation accompanying electron transfer.<sup>8</sup> Yet, it does not account for the quantum mechanical nature of the electron propagation and the nuclear dynamics that underlies the structural reorganisation. In this Article, we develop a fully quantum mechanical treatment of these interactions. This approach, combined with DFT calculations and experimental transport studies of the sequential tunnelling regime of single-molecule junctions, is used to understand the mechanism of electron transfer on a single-molecule scale.

## Results and discussion

The device architecture we use as a platform to study electron transfer is shown schematically in Figure 1a, and is described in detail in the SI. Briefly, we fabricate graphene nanogaps that comprise pairs of source and drain electrodes spaced by 1–2 nm using feedback-controlled electroburning.<sup>9-12</sup> Zinc porphyrin molecules, functionalised with anchor groups designed to bind to the graphene electrodes via  $\pi$ - $\pi$  stacking (Figure 1b), are deposited from solution. A gate electrode is used to adjust the energy of the molecular levels relative to the Fermi levels of the source and drain electrodes. The gate electrode is crucial as it allows us to investigate resonant transport, and therefore electron transfer, in our molecular junctions. Figure 1c shows a low-temperature (3.5 K) conductance map for such a device (device **A**) measured as a function of bias and gate voltage. Within most of the map the current is Coulomb blocked, indicating that  $\pi$ - $\pi$  stacking leads to weak molecule-electrode coupling. In addition, we observe a high conductance region in which sequential electron transfers take place. We further observe lines of increased conductance running parallel to the edges of the high-current region. Previous studies have assigned such conductance lines to vibrational excitations of the molecule during the charging process. At

low bias resonant transfer occurs between the vibrational ground states of both charge states. As the bias voltage is increased, electron transfer onto the molecule can be accompanied by a vibrational excitation.<sup>13-15</sup> This interpretation is substantiated by the fact that the average spacing between the lines measured for device **A** corresponds to  $4.9 \pm 0.3$  meV, which is in close agreement with the only strongly-coupled low-lying vibrational mode of the molecule predicted by DFT calculations (6.0 meV, see SI). Furthermore, the same mode is independently found in another device (see SI). In order to account for the observed behaviour, we describe the charge transport through the junction as a sequence of reduction and oxidation reactions occurring at the source and drain electrodes. The rates of these reactions depend on the interaction between the electronic and vibrational degrees of freedom of the molecule and its environment as illustrated in Figure 1d.

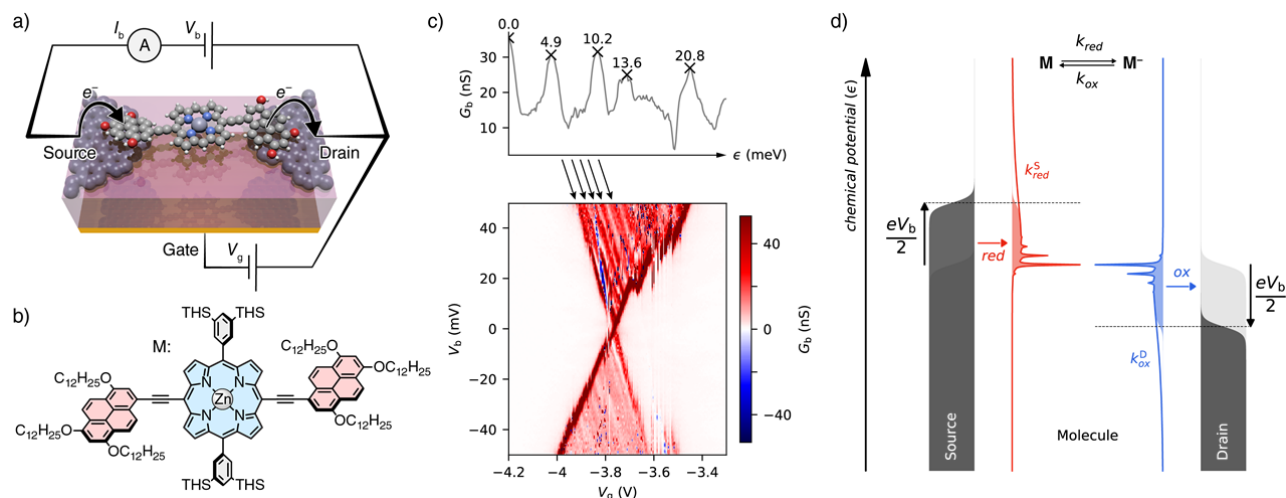


**Figure 1.** a) Schematic representation of our device architecture: nanometre-separated graphene source and drain electrodes are used to contact the redox-active molecule, and a local gate electrode separated from the molecule by a thin layer of HfO<sub>2</sub> (10 nm thick) is used to shift the molecular energy-levels. b) The molecule **M** used in this study comprises of a redox-active porphyrin core (blue), with solubilising aryl side-groups on two of the porphyrin *meso*-positions (grey), and  $\pi$ -stacking anchor groups on the other two *meso*-positions (red); here TMS is trihexylsilyl. c) Charge stability diagram showing the differential conductance ( $G_b$ ) as a function of bias voltage ( $V_b$ ) and gate voltage ( $V_g$ ) at 3.5 K; the actual gate voltage experienced by the molecule is only a fraction of the applied gate voltage because of the drop across the HfO<sub>2</sub> layer. The top panel shows the differential conductance of the top triangle as an average along the lines indicated by the arrows running parallel to the edge of the triangle. d) Schematic representation of current flowing through our single-molecule transistor. The energy-dependent reduction and oxidation rate constants are shown in red and blue, respectively, with electron-transfer rates shown as coloured areas. The Fermi-Dirac distributions  $f_s$  and  $f_d$ , are shown as the grey areas for source and drain, respectively. At negative bias voltage, electrons tunnel sequentially from the source via the molecule into the drain. For convenience, the bias voltage is drawn as applied symmetrically across the source and drain electrodes.

The general expression (quantum master equation, QME) for the net current is given by<sup>16-18</sup>

$$I = |e| \frac{\gamma_{ox}^S \gamma_{red}^D - \gamma_{red}^S \gamma_{ox}^D}{\gamma_{red}^S + \gamma_{red}^D + \gamma_{ox}^S + \gamma_{ox}^D}, \quad (1)$$

where  $e$  is the elementary charge. The electron-transfer rates for each electrode (S/D) are given by equations **2** and **3**:

$$\gamma_{red} = (2 - \Omega) \int f(\epsilon) k_{red}(\epsilon) d\epsilon, \quad (2)$$

$$\gamma_{ox} = (1 + \Omega) \int (1 - f(\epsilon)) k_{ox}(\epsilon) d\epsilon, \quad (3)$$

where  $f(\epsilon)$  is the Fermi-Dirac distribution, and  $k_{red/ox}$  are the (energy-dependent) rate constants for the corresponding electron-transfer reactions. The current-voltage trace of device **A**, measured on resonance (Figure 2a) reveals an asymmetry between the current at positive and negative bias voltages. This is a direct result of electron-electron interactions in the presence of asymmetric molecule-electrode couplings and spin degeneracy. If tunnelling occurs into an unoccupied orbital (LUMO) (e.g. the  $N/N+1$  transition, where  $N$  is the number of electrons on the molecule in the neutral state) two possible pathways exist for reduction – an electron of either spin can tunnel from the electrode onto the molecule. Only one possible path exists for the oxidation reaction as the unpaired electron (in what is now the SOMO) tunnels out of the molecule and into the electrode. Conversely, if tunnelling occurs into a singly occupied orbital (e.g. the  $N-1/N$  transition) the opposite is the case: only electrons of the opposite spin to that on the molecule can reduce the molecule, but electrons of either spin can oxidise the neutral molecule. The number of possible transitions is accounted for by setting  $\Omega$  to 0 for the  $N/N+1$  transition or 1 for the  $N-1/N$  transition. The current asymmetry with respect to the sign of the bias voltage cannot be observed in non-interacting (Landauer) systems, i.e. off-resonance or in the case of strong coupling between the molecule and the electrodes (where the energy uncertainty associated with the lifetime of the electronic states is greater than the energy required to change the charge state of the molecule).

The energy-dependent rate constants ( $k_{red/ox}$ ) are determined by the molecule-electrode interactions, as well as by structural reorganisation of the molecule upon electron transfer. Previous studies have estimated these functions based on the Franck-Condon factors of a single vibrational mode with limited success.<sup>13,15,19</sup> These

studies ignored the fact that the time-energy uncertainty relationship results in lifetime broadening of the electronic states. Moreover, recent experimental studies have shown a significant contribution from the dielectric substrate to the reorganisation energy of single molecules.<sup>20</sup> We account for both lifetime broadening and the influence of the environment in our expression for the rate constants<sup>17</sup>

$$k(\epsilon) = \frac{1}{\pi} \text{Re} \left[ \Gamma_{S/D} \int e^{\sigma i(\epsilon - \mu)t} e^{-t/\tau} B(t) dt \right], \quad (4)$$

where  $\Gamma_{S/D}$  is the electronic coupling to the source/drain electrode,  $\tau = 2(\Gamma_S + \Gamma_D)^{-1}$  is the lifetime of the electronic state, and  $\mu$  the energy level of the molecule. The sign  $\sigma$  is either 1 for reduction or  $-1$  for oxidation. The phononic correlation function,  $B(t)$ , which can be thought of as a time-dependent Frank Condon factor that describes the nuclear dynamics accompanying electron transfer,<sup>21</sup> is given by:

$$B(t) = \exp \left[ \int \frac{J(\omega)}{\omega^2} \left( \coth \left( \frac{\omega}{2k_B T} \right) \times (\cos \omega t - 1) - i \sin \omega t \right) d\omega \right], \quad (5)$$

where  $J(\omega) = \sum_q |g_q|^2 \delta(\omega - \omega_q)$  is the spectral density for phonons and vibrations with frequencies  $\omega_q$  and electron-phonon coupling strengths  $g_q$ ;  $k_B T$  is the thermal energy. We began by fitting the differential conductance of device **A** on resonance to equation 1, Figure 2a (bottom panel), with  $\Gamma_S$ ,  $\Gamma_D$ ,  $\omega_q$  and  $g_q$  as the fitting parameters. We found that the low-bias electron transfer is dominated only by a single molecular vibrational mode with energy  $\hbar\omega_q = 4.2$  meV and Huang-Rhys parameter  $S_q = g_q^2 / \hbar^2 \omega_q^2 = 0.4$ . However, a spectral density consisting of only this single mode cannot fully reproduce the experimental data. Only if we include a structureless super-Ohmic background<sup>22</sup> accounting for the coupling to the substrate, do we find a good agreement with the empirical data, as shown in Figure 2a (top panel). The complete fit therefore comprises two additional parameters to describe the environment: the corresponding reorganisation energy,  $\lambda_o$ , and the average phonon frequency  $\langle \omega_o \rangle$ . From the fit we obtain  $\lambda_o = 26$  meV and  $\hbar \langle \omega_o \rangle = 25$  meV. The spectral density therefore contains both an inner sphere contribution, corresponding to structural reorganisation of the molecule, and an outer sphere contribution from the surrounding dielectric environment. Molecule-electrode coupling leads to a lifetime broadening of the conductance peaks:  $\hbar/\tau = 0.31$  meV. Omitting lifetime broadening leads to a  $\sim 30\%$  overestimation of the zero-bias conductance (see SI). The validity of our approach is further substantiated by the fact that using the parameters obtained from fitting a single differential conductance trace on resonance,

we can calculate the entire current map as function of bias and gate voltage which shows excellent agreement with the experimental data, as shown in Figure 2b. Moreover, we can successfully fit the resonant current-voltage traces between 5 K and 70 K with the above spectral density (Figure 3a) using the same phononic parameters:  $\omega_q$ ,  $g_q$ ,  $\lambda_o$  and  $\langle\omega_o\rangle$ . Importantly, we find that at elevated temperature (above 20 K), the details of the spectral density are lost in the  $IV$ -characteristics due to thermal broadening.

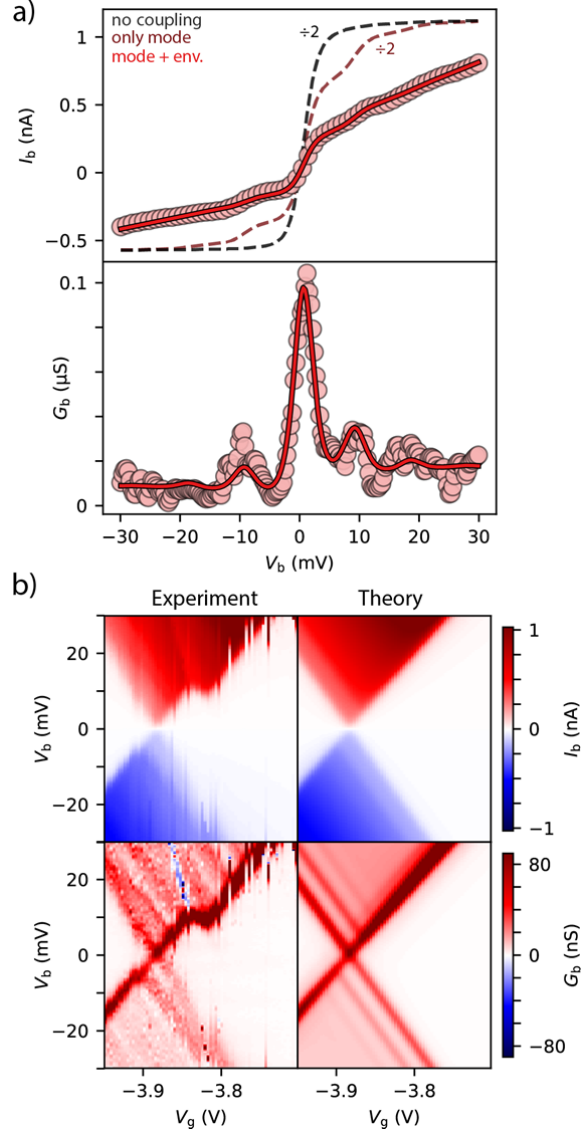


**Figure 2.** a) Current ( $I_b$ ) and differential conductance ( $G_b$ ) as a function of bias voltage ( $V_b$ ) of device **A** (circles) at 5 K, corresponding fit to our model (red line), and corresponding curves without environmental coupling (dark red line) or without vibrational coupling (black line). b) Experimental current (left top) and differential conductance (left bottom) maps as a function of bias and gate voltage of device **A**, and reconstructed maps (right) from the parameters used to fit the  $IV$  trace in a).

Since in the  $IV$  curves in Figure 3a show that above 20 K we no longer observe the presence of individual vibrational modes, we proceed to examine the suitability of semi-classical Marcus Theory (MT) for describing electron transfer in our devices. MT can be recovered as the high temperature limit ( $k_B T \gg \hbar\langle\omega\rangle, \hbar/\tau$ ) of our QME model (see SI) with rate constants in equation 4 simplifying to the familiar form:<sup>23-25</sup>

$$k(\epsilon) = \Gamma_{S/D} \sqrt{\frac{1}{4\pi\lambda k_B T}} \exp\left[-\frac{(\lambda \pm (\epsilon - \mu))^2}{4\lambda k_B T}\right], \quad (6)$$

where  $\lambda = \lambda_i + \lambda_o$  is the total reorganisation energy. We compare the performance of MT with our QME model for 3 devices, **B–D** (fabricated with a 300 nm SiO<sub>2</sub> gate dielectric, see SI), measured at 77 K. Since devices **B–D** were measured within a larger bias voltage range it is now necessary to incorporate all of the molecular vibrational modes in the QME analysis of the electron transport. Therefore, in what follows, the overall spectral density in equation 5 comprises all molecular vibrational modes as well as a broad background which phenomenologically accounts for the dielectric substrate:

$$J(\omega) = \sum_q |g_q|^2 \delta(\omega - \omega_q) + J_{bg}(\omega), \quad (7)$$

The frequencies and coupling strengths of the molecular modes were calculated using DFT and correspond to an inner-sphere reorganisation energy of  $\lambda_i = \hbar \sum_q \omega_q S_q$  of 67 meV (see SI for details) whereas the background is again modelled as a structureless super-Ohmic spectral density. These outer and inner-sphere contributions are plotted in Figure 3b. Figure 3c shows the comparison between the QME and MT reduction rates calculated for the instructive values of  $\lambda$ . It demonstrates that at 77 K, and indeed even at room temperature, the QME rate constants extend over a broader energy range than their Marcus counterparts as they take into account molecular vibrations from low-energy bending motion (a few meV) to  $sp^2$  C-C bond stretches ( $\sim 200$  meV). Unlike the Marcus rates, they are also not symmetric around  $\epsilon = \lambda$ .

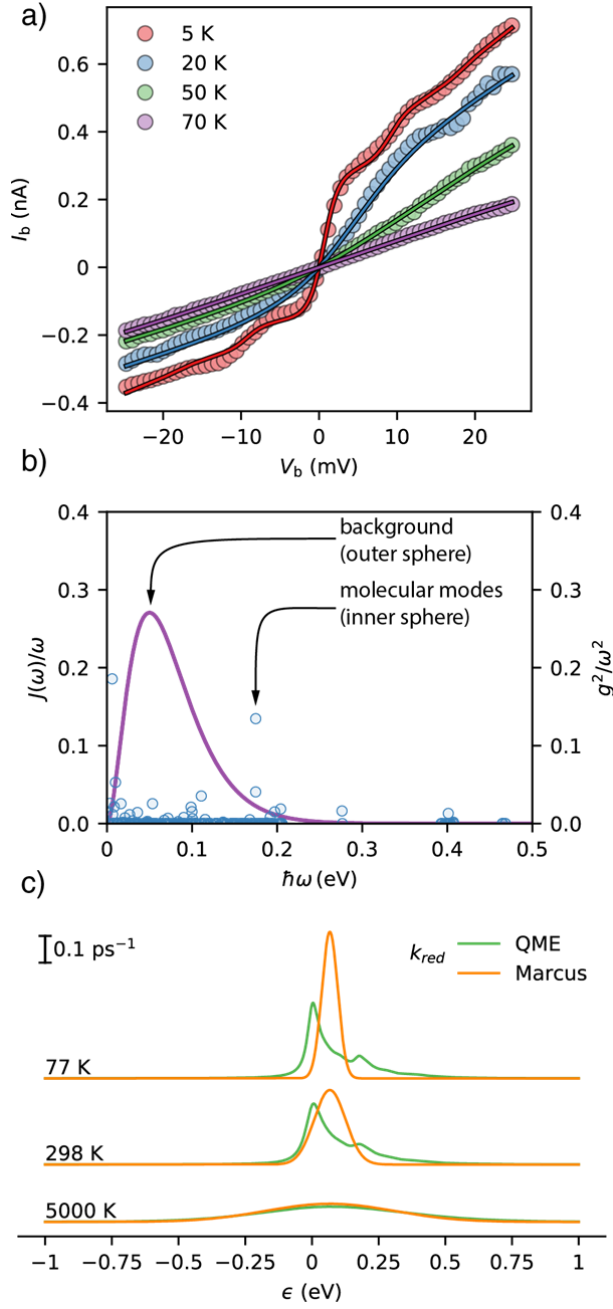


**Figure 3** a)  $IV$  traces of device **A** at various temperatures (circles) and the global fit (solid lines) where all parameters except the molecule-electrode couplings are shared. b) Spectral density used for the QME model consisting of a background and individual molecular modes calculated by DFT. Background parameters:  $\lambda_o = 25$  meV,  $\omega_o = 25$  meV. c) Calculated reduction rate constant at the drain electrode as a function of chemical potential for 3 different temperatures for the QME model and Marcus theory. Parameters (QME:  $\lambda_o = 25$  meV,  $\omega_o = 25$  meV,  $\lambda_i = 67$  meV; Marcus:  $\lambda = 92$  meV) were chosen to emphasise the difference between the two models at low  $\epsilon$ .

We find that our experimental charge transport data are not adequately described by MT, as shown in Figure 4 for devices **B–D**.<sup>26</sup> In particular the data show the conductance at low-bias voltages is severely underestimated since MT treats the nuclear dynamics classically. At low bias voltages, the barrier for electron tunnelling cannot be



overcome solely due to thermal fluctuations of the environment, resulting in very low electron transfer rates. Quantum mechanically, however, electron transfers at low bias are dominated by nuclear quantum mechanical tunnelling (i.e. overlap between the vibrational wavefunctions in the classically forbidden region) and consequently electron transfer can occur relatively efficiently. This shortcoming of MT can be partially mitigated by expanding the phonon correlation function to higher order,<sup>17,27</sup> or by coarse-graining low- ( $\hbar\omega_q \ll kT$ ) and high-energy ( $\hbar\omega_q \gg kT$ ) vibrational modes as is done in the Marcus-Levich-Jortner theory.<sup>27,28</sup> As shown in the SI, such approaches partially rectify some of the shortcomings of MT, highlighting the non-classical mechanism of electron transfer even in these relatively high-temperature conditions. Our experimental data, however, are best described by our fully quantum mechanical treatment involving both inner and outer sphere reorganisation, as discussed above. The current–voltage traces of devices **B–D** in Figure 4a are therefore fitted using the QME approach and with spectral density given in equation 6, treating  $\Gamma_S$ ,  $\Gamma_D$  and  $\lambda_o$  as free fitting parameters (see SI section 5 and 8). We obtain outer-sphere reorganisation energies of  $\lambda_o = 180, 240$  and  $220$  meV for devices **B–D**, respectively. We assign the relatively large variation in outer-sphere reorganisation energy to small variations in the distance of the porphyrin from the dielectric surface. In the SI, by modelling the porphyrin as a rectangle with uniformly distributed charge, we estimate that the above values of  $\lambda_o$  correspond to the porphyrin molecules being roughly 0.71, 0.51 and 0.58 nanometres away from the dielectric substrate, respectively (Figure 4c, see SI for details of the calculation).<sup>20,29</sup> In addition, in the SI we present data for 9 additional devices, comprising porphyrin molecules that differ only by the  $\pi$ -anchoring group. The values of  $\lambda_o$  obtained for these devices are in the range of 110 – 250 meV. These results emphasise the importance of the broader molecular environment, since even in our simple device-architecture, small changes in the molecule-substrate distance lead to large changes in reorganisation energy. This in turn results in significant variations in the electron-transfer rates.

It is becoming clear that the molecular environment is a key factor in controlling charge-transfer reactions in Natural processes, such as photosynthesis and oxidative phosphorylation.<sup>2</sup> Our results support the findings that an enzymatic environment is more than simply a template to pre-organise reagents, but it likely provides an optimised outer-sphere reorganisation energy to maximise the efficiency of redox processes. One can envisage biomimetic strategies for controlling the molecular environment, and therefore electron-transfer rates, in fabricated devices, based on well-developed chemical methods of supramolecular assembly.<sup>30</sup>

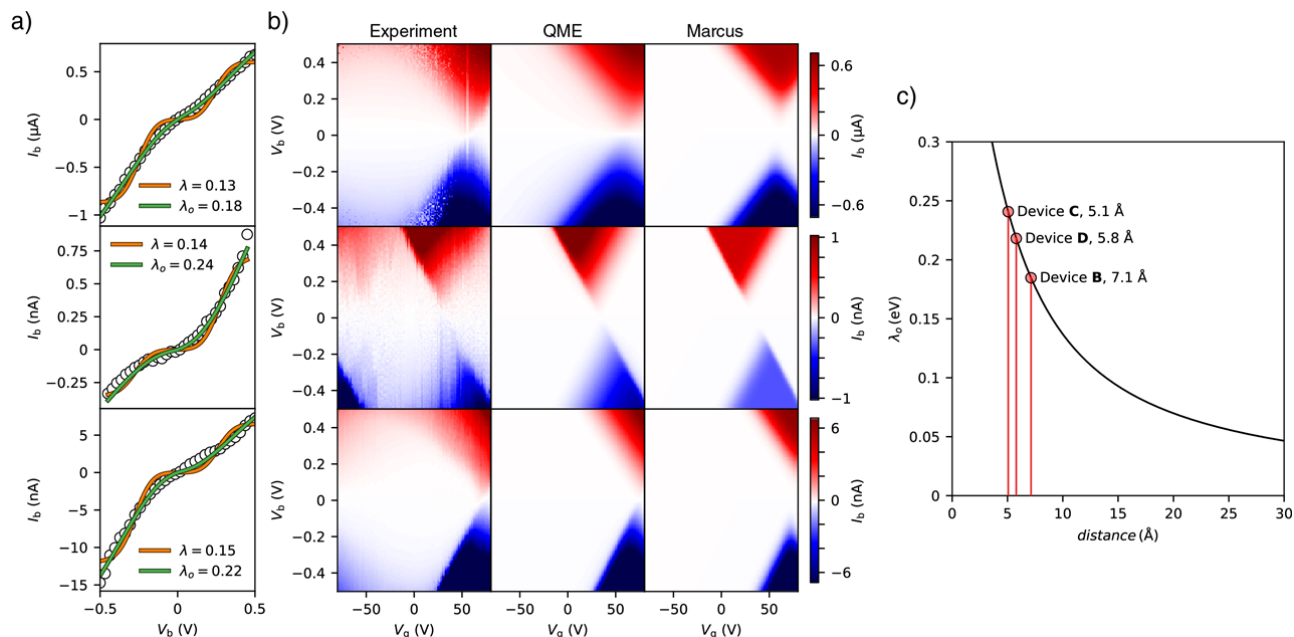


**Figure 4.** a)  $IV$  traces at resonance of 3 devices (**B**, **C**, **D**) of molecule **M** at 77 K (data from ref <sup>26</sup>) and the fit to the Marcus model (orange) and the QME model (green). For clarity, fewer experimental data-points were shown. b) Charge stability diagrams of the same 3 devices as in c, and the reconstructed stability diagrams from the fits in c according the QME model, or the Marcus model. c) The molecule–dielectric distance calculated for **B–D** from fitted values of  $\lambda_o$  (see SI for details).

## Conclusions

The ability to probe energy-dependent single-electron-transfer rates down to the level of an individual molecule has provided us with a platform to fully uncover the role of environmental interactions in electron transfer in molecular systems and examine the validity of various electron-transfer theories. We have demonstrated that, as a result of strong electron-vibrational interaction, electron transfer can take place over a broad range of electron energies determined by an inner and outer sphere structural reorganisation energy, leading to a gradual increase in the current  $\lambda$  as a function of bias voltage. This is a marked difference from non-interacting systems, where the current increases in a step-wise fashion. We have further shown that it is necessary to account for the quantum-mechanical nature of vibrational dynamics throughout the experimentally relevant temperature range. Marcus theory fails to adequately describe the low-bias transport behaviour due to the typically large energy range of molecular vibrations (up to 400 meV) and the high-temperature assumptions behind thermally activated transport.

Our fully quantum-mechanical description of electron transfer which, besides the electron-vibrational interactions, also accounts for lifetime broadening and spin-degeneracy of the electronic levels yields an excellent agreement with the experimental data and should be broadly applicable in fundamental studies of electron transfer, especially in the field of molecular electronics. Our results further demonstrate the importance of precisely controlling the molecular environment in designing functional molecular technologies including molecular transistors, thermoelectric materials and biomimetic systems for light-to-electricity energy conversion. Finally, we have shown that single-molecule junctions can act as a novel tool to unravel the mechanism of electron transfer in molecular systems. This opens the door towards investigations of mechanisms of electron transport within extended molecular systems as well as photo-induced electron transfer, and thus shedding further light on some of the most important phenomena in chemistry.

## Acknowledgements

The authors thank G. Holloway for developing the method to fabricate the 3-terminal electrode design. This work was supported by the EPSRC (grants EP/N017188/1 and EP/R029229/1). J.K.S. thanks the Clarendon Fund, Hertford College and EPSRC for financial support. E.M.G. acknowledges funding from the Royal Society of Edinburgh and the Scottish Government, J.A.M. acknowledges funding from the Royal Academy of Engineering.

## Author contributions

J.O.T., B.L., J.K.S., H.L.A and J.A.M. guided the study. J.O.T. synthesised compound **M**. J.O.T. and B.L. performed graphene transfer and patterning, cryogenic measurements and data analysis. J.O.T. performed DFT calculations. B.L. and J.K.S. fitted the data. J.K.S. and E.M.G. developed the theory and fitting models. K.W. fabricated the substrates under supervision of J.B.. All authors contributed to writing and editing the manuscript.

## References

- 1 Brookes, J. C. Quantum effects in biology: golden rule in enzymes, olfaction, photosynthesis and magnetodetection. *Proc. R. Soc. A* **473**, 20160822, (2017).
- 2 Sjulstok, E., Olsen, J. M. H. & Solov'yov, I. A. Quantifying electron transfer reactions in biological systems: what interactions play the major role? *Sci. Rep.* **5**, 18446, (2015).
- 3 de Nijs, B. *et al.* Plasmonic tunnel junctions for single-molecule redox chemistry. *Nat. Commun.* **8**, 994, (2017).
- 4 Josefsson, M. *et al.* A quantum-dot heat engine operating close to the thermodynamic efficiency limits. *Nat. Nanotechnol.*, **13** 920-924 (2018).
- 5 Foster, S. L. *et al.* Catalysts for nitrogen reduction to ammonia. *Nat. Catal.* **1**, 490-500, (2018).

- 6 Sokol, K. P. *et al.* Bias-free photoelectrochemical water splitting with photosystem II on a dye-sensitized photoanode wired to hydrogenase. *Nat. Energy*, <https://doi.org/10.1038/s41560-018-0232-y> (2018).
- 7 Landauer, R. Spatial Variation of Currents and Fields Due to Localized Scatterers in Metallic Conduction. *IBM J. Res. Dev.* **1**, 223-231, (1957).
- 8 Migliore, A., Schiff, P. & Nitzan, A. On the relationship between molecular state and single electron pictures in simple electrochemical junctions. *Phys. Chem. Chem. Phys.* **14**, 13746-13753, (2012).
- 9 El Abbassi, M. *et al.* From electroburning to sublimation: substrate and environmental effects in the electrical breakdown process of monolayer graphene. *Nanoscale* **9**, 17312-17317, (2017).
- 10 Prins, F. *et al.* Room-temperature gating of molecular junctions using few-layer graphene nanogap electrodes. *Nano Lett.* **11**, 4607-4611, (2011).
- 11 Xu, Q. *et al.* Single Electron Transistor with Single Aromatic Ring Molecule Covalently Connected to Graphene Nanogaps. *Nano Lett.* **17**, 5335-5341, (2017).
- 12 Lau, C. S., Mol, J. A., Warner, J. H. & Briggs, G. A. D. Nanoscale control of graphene electrodes. *Phys. Chem. Chem. Phys.* **16**, 20398-20401, (2014).
- 13 Lau, C. S. *et al.* Redox-Dependent Franck–Condon Blockade and Avalanche Transport in a Graphene–Fullerene Single-Molecule Transistor. *Nano Lett.* **16**, 170-176, (2016).
- 14 Burzurí, E. *et al.* Franck–Condon Blockade in a Single-Molecule Transistor. *Nano Lett.* **14**, 3191-3196, (2014).
- 15 Burzurí, E. *et al.* Sequential Electron Transport and Vibrational Excitations in an Organic Molecule Coupled to Few-Layer Graphene Electrodes. *ACS Nano* **10**, 2521-2527, (2016).
- 16 Galperin, M., Mark, A. R. & Abraham, N. Molecular transport junctions: vibrational effects. *J. Phys.: Condens. Matter* **19**, 103201, (2007).
- 17 Sowa, J. K., Mol, J. A., Briggs, G. A. D., Gauger, E. M. Beyond Marcus theory and the Landauer–Büttiker approach in molecular junctions: A unified framework. *J. Chem. Phys.*, <https://dx.doi.org/10.1063/1.5049537> (2018).
- 18 Zhang, J. *et al.* Single-Molecule Electron Transfer in Electrochemical Environments. *Chem. Rev.* **108**, 2737-2791, (2008).
- 19 Braig, S. & Felnsberg, K. Vibrational sidebands and dissipative tunneling in molecular transistors. *Phys. Rev. B* **68**, 205324, (2003).
- 20 Fatayer, S. *et al.* Reorganization energy upon charging a single molecule on an insulator measured by atomic force microscopy. *Nat. Nanotechnol.* **13**, 376-380, (2018).
- 21 Todd, M. D., Nitzan, A., Ratner, M. A. & Hupp, J. T. Electron transfer rates from time-dependent correlation functions. Wavepacket dynamics, solvent effects, and applications. *J. Photochem. Photobiol. A* **82**, 87-101, (1994).
- 22 Weiss, U. *Quantum Dissipative Systems*. (WORLD SCIENTIFIC, 2011).
- 23 Chidsey, C. E. D. Free Energy and Temperature Dependence of Electron Transfer at the Metal-Electrolyte Interface. *Science* **251**, 919-922, (1991).
- 24 Marcus, R. A. & Sutin, N. Electron transfers in chemistry and biology. *Biochimica et Biophysica Acta (BBA) - Reviews on Bioenergetics* **811**, 265-322, (1985).
- 25 Yuan, L. *et al.* Transition from direct to inverted charge transport Marcus regions in molecular junctions via molecular orbital gating. *Nat. Nanotechnol.* **13**, 322-329, (2018).
- 26 Limburg, B. *et al.* Anchor Groups for Graphene-Porphyrin Single-Molecule Transistors. *Adv. Funct. Mater.* 1803629, (2018).
- 27 Devault, D. Quantum mechanical tunnelling in biological systems. *Q. Rev. Biophys.* **13**, 387-564, (2009).
- 28 Jortner, J. Temperature dependent activation energy for electron transfer between biological molecules. *J. Chem. Phys.* **64**, 4860-4867, (1976).
- 29 Iván, S. & Mats, P. Frontier molecular orbitals of a single molecule adsorbed on thin insulating films supported by a metal substrate: electron and hole attachment energies. *J. Phys.: Condens. Matter* **29**, 355002, (2017).
- 30 Milan, D. C. *et al.* The single-molecule electrical conductance of a rotaxane-hexayne supramolecular assembly. *Nanoscale* **9**, 355-361, (2017).